Optimization and Modeling of the Crystallization Process in a Cascade with Backmixing

Pieter J. Jansens, Odolphus S. L. Bruinsma, and Gerda M. van Rosmalen
Delft University of Technology, Laboratory for Process Equipment,
Leeghwaterstraat 44, 2628 CA Delft, The Netherlands

Cascades of crystallizers are applied in many industrial processes. The optimization of the filterability of crystals produced in such a cascade is dealt with, since a good filterability is often one of the main product specifications. An integral model description of the crystallization process is developed that allows for the prediction of the crystal size distribution and the filterability in each stage of the cascade, and experiments are performed to support this model. The integral model can be used as a predictive tool in future filterability optimization studies.

Introduction

Fractional suspension crystallization processes are aimed at ultrapurification of organic compounds and are based on cooling crystallization (Zief and Wilcox, 1967). These processes generally comprise a cascade of crystallizers and a downstream solid/liquid separation unit (Jansens and Van Rosmalen, 1994). The overall separation efficiency of these processes depends to a large extent on the filterability of the crystals produced in the cascade.

This article is focused on optimization of the crystallization process in cascades of crystallizers, primarily with respect to the filterability of the product crystals. Optimization and control of the product filterability requires a good understanding of the hydrodynamics and the crystallization process in the cascade. Therefore this study is also aimed at the development of an integral model description of the crystallization process in cocurrent cascades, which can be a useful tool in the filterability optimization process.

A series of experiments was conducted to determine the effect of practical process variables (throughput, feed temperature and composition, and coolant flow and temperature) on the permeability of the crystals in the different compartments and in the product outlet in a pilot-scale cascade of crystallizers. The permeability of a bed of crystals is a quantitative measure of the filterability of these crystals. The experiments were performed with a so-called cooling disc crystallizer (CDC), which can be regarded as an *integrated cascade* featuring a concurrent contact between the crystals and the mother liquor with *backmixing* between the compartments. The pilot CDC (Figure 1) consists of a horizontal trough that is divided into eight compartments by seven fixed cooling elements. In each compartment a disc equipped with wipers and mixing blades slowly rotates. The product slurry flows from one compartment to the next via small openings at the bottom of the cooling elements and leaves the CDC by an overflow in the last compartment. The CDC was selected for this study because of two characteristics that were expected to have a beneficial impact on the filterability of the product crystals: (1) the complete absence of auxiliary slurry transport equipment, and (2) its ability to operate with very high crystal contents (up to 45 vol. %).

Along with the experimental program, a mathematical description of the crystallization process in a cocurrent cascade

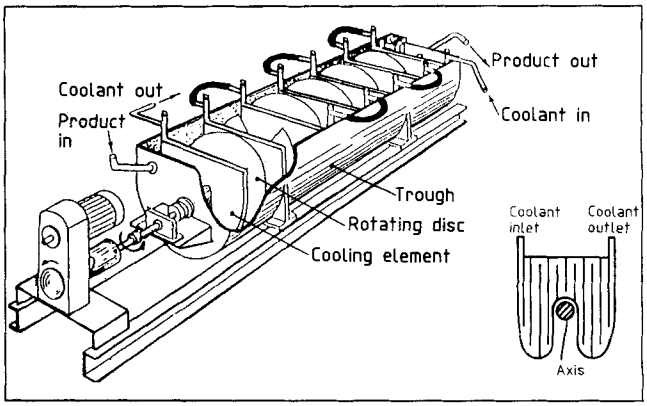

Figure 1. Cooling disc crystallizer (GMF-Gouda) with a detail of cooling element.

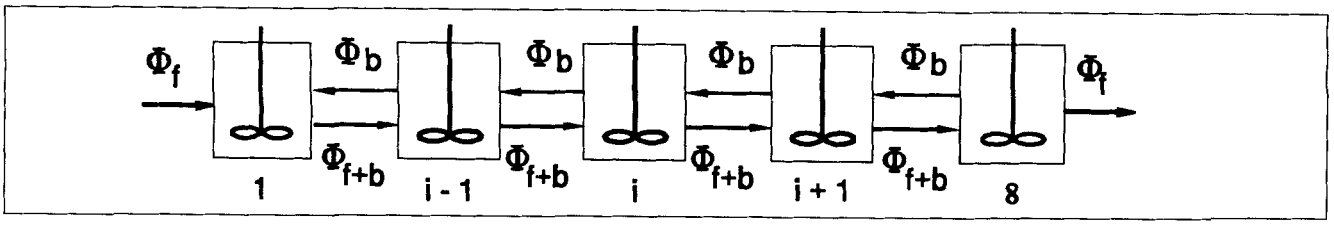

Figure 2. Cascade with backmixing model (8 compartments).

of crystallizers with backmixing (CCB) has been developed. The CCB model integrates five aspects: (i) hydrodynamics, (ii) mass and heat transfer, (iii) thermodynamics and crystallization kinetics, (iv) crystal size distribution (CSD), and (v) bed porosity and permeability. Key parameters in the model are a backmix ratio, a classification ratio, a nucleation constant, and a nucleation exponent. The integral model description allows for the calculation of the CSD, the nucleation rate, the growth rate, and the permeability of the crystals in every compartment and in the product outlet of a cascade of crystallizers.

The importance of this contribution is that it links operating conditions to the most relevant properties of a crystalline product (CSD and filterability) by a combination of mass, heat, and population balances. Further, this is the first example in which population densities of crystal slurries are directly translated into the porosity and permeability of a bed of these crystals. It is stressed here that the model is of general importance and its use is not restricted to the CDC.

Model Formulation

Hydrodynamics

The hydrodynamics of stirred tanks with backmixing has been investigated extensively by Van der Laan (1958), Bell and Babb (1965), Klinkenberg (1968), and Roemer and Durbin (1967). Roemer and Durbin presented the backflow cell (BC) model, which consists of N ideally mixed cells of equal volume with a constant net throughput Φ_f and with equal backmix flow Φ_b between neighboring cells (see Figure 2).

The residence time distribution function $E(t)$ for a single-phase flow through this cascade reads:

$$E(t) = \sum_{m=1}^{N} \frac{A_m}{\tau} \exp\left(s_m \frac{t}{\tau}\right) \tag{1}$$

where A_m and S_m are complex functions depending on the backmix ratio f and on the number of cells N (Roemer and Durbin, 1967).

$$f = \frac{\Phi_b}{\Phi_f}. \tag{2}$$

The backmix ratio can be calculated from the mean residence time and the variance of an experimentally determined residence time distribution curve (Van der Laan, 1958):

$$\frac{\sigma^2}{\tau^2} = \frac{N(1-F^2) - 2F(1-F^N)}{N^2(1-F^2)} \quad \text{and} \quad F = \frac{f}{1+f}. \tag{3}$$

Bell and Babb (1965) argue that the BC model can also be applied to multiphase flow cases, provided that all phases are well mixed. In the case of crystallization of organics from the melt this condition is nearly always satisfied because the difference in specific weight between the crystals and their mother liquor is usually small. Hence, the BC model can be used to describe the hydrodynamic behavior of a cascade of crystallizers. Typical of the CDC is the removal of product via an overflow that may cause some classification in the last compartment. For this purpose a *size-independent* classification ratio h is included in the hydrodynamic model. From this assumption it follows:

$$h = \frac{w_{\text{overflow}}}{w_{\text{comp.}N}}. \tag{4}$$

If the last compartment of a cascade is a mixed-product removal-type crystallizer, the value of h is 1.

Mass and heat transfer

Assuming that the formed solid phase is 100 percent pure, the component balances over compartments 1, i, and N of a cascade of crystallizers can be reduced to Eqs. 5, 6, and 7:

$$x_f + f*[w_2 + (1-w_2)*x_2] - (1+f)*[w_1 + (1-w_1)*x_1] = 0, \tag{5}$$

$$(1+f)*[w_{i-1} + (1-w_{i-1})*x_{i-1}] + f*[w_{i+1} + (1-w_{i+1})*x_{i+1}] - (1+2f)*[w_i + (1-w_i)*x_i] = 0, \tag{6}$$

$$(1+f)*[w_{N-1} + (1-w_{N-1})*x_{N-1}] - f*[w_N + (1-w_N)*x_N] - h*w_N - (1-h*w_N)*x_N = 0. \tag{7}$$

The heat of crystallization and the sensible heat are removed through the coolant. A heat balance on the coolant side over compartment i yields

$$\Phi_c * C_{p,c} * (T_{c,i} - T_{c,i+1}) - K * A * (\Delta T)_{cp,i} = 0. \tag{8}$$

For the cooling element i, which separates compartments i and $i+1$, $(\Delta T)_{cp,i}$ is simply defined as

$$(\Delta T)_{cp,i} = \frac{1}{2} * \left(T_{p,i} - \frac{T_{c,i} + T_{c,i+1}}{2}\right) + \frac{1}{2} * \left(T_{p,i+1} - \frac{T_{c,i} + T_{c,i+1}}{2}\right). \tag{9}$$

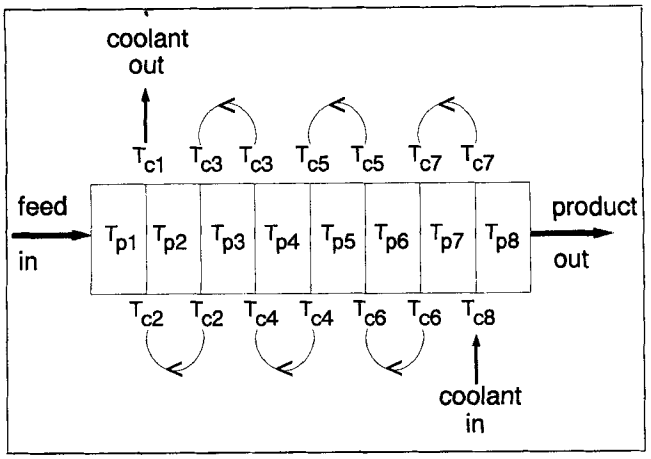

Figure 3. Definition/numbering of the temperature of product slurry (T_p) and coolant (T_c) in the pilot CDC with 8 compartments.

The numbering of T_p and T_c is illustrated in Figure 3.

Assuming that heat transfer to the environment is negligible, heat balances on the product side over compartments 1, i, and N can be reduced to Eqs. 10, 11, and 12:

$$H_{\text{feed}} + f * H_{SL,2} - (1+f) * H_{SL,1} - \frac{K * A}{\Phi_f} * (\Delta T)_{pc,1} = 0, \tag{10}$$

$$(1+f) * H_{SL,i-1} + f * H_{SL,i+1} - (1+2f) * H_{SL,i} - \frac{K * A}{\Phi_f} * (\Delta T)_{pc,i} = 0, \tag{11}$$

$$(1+f) * H_{SL,N-1} - f * H_{SL,N} - h * w_N * H_{S,N} - (1 - h * w_N) * H_{S,N} - \frac{K * A}{\Phi_f} * (\Delta T)_{pc,N} = 0. \tag{12}$$

For compartment i, $(\Delta T)_{pc,i}$ is defined as

$$(\Delta T)_{pc,i} = \frac{1}{2} * \left(T_{p,i} - \frac{T_{c,i-1} + T_{c,i}}{2} \right) + \frac{1}{2} * \left(T_{p,i} - \frac{T_{c,i+1} + T_{c,i}}{2} \right). \tag{13}$$

In conventional cascades consisting of separate vessels equipped with cooling jackets the terms $(\Delta T)_{cp,i}$ and $(\Delta T)_{pc,i}$, which represent the local temperature difference between the coolant and the product, are identical. In the CDC, however, $N-1$ cooling elements separate N compartments (see Figures 1 to 3). Obviously, the fact that in a CDC the first and the last compartment face only one side of a cooling element must be accounted for in the calculations.

The enthalpy of the liquid phase is assumed to be independent of its concentration and is defined as zero at the melting point of the pure main component. The enthalpies of the slurry (H_{SL}), the liquid phase (H_L), and the solid phase (H_S) are defined as

$$H_{SL,i} = w_i * H_{S,i} + (1 - w_i) * H_{L,i}, \tag{14}$$

$$H_{L,i} = C_{p,L} * (T_{p,i} - T_m), \tag{15}$$

$$H_{S,i} = -\Delta H_m + C_{p,L} * (T_{p,i} - T_m). \tag{16}$$

Thermodynamics and kinetics

Each compartment of the cascade is assumed to be a class II crystallizer, which means that the yield is independent of the throughput, and the exit concentration of the liquid phase approaches the equilibrium concentration (Randolph and Larson, 1988). Thus the liquid concentration in each compartment can be calculated using a relation for the liquidus curve. Here, for the sake of simplicity, the liquidus is described as a straight line with slope q:

$$x_i = 1 - \frac{(T_m - T_{p,i})}{q}. \tag{17}$$

Randolph and Larson suggest the following empirical correlation for the nucleation rate in mixed suspension crystallizers:

$$B = k(T) * \omega^x * w^y * s^z, \tag{18}$$

where ω is a measure for the mechanical agitation, w is the crystal content or suspension density, and s is the degree of supersaturation. The exponent y in Eq. 18 is usually 1 (Garside and Shah, 1980). In a class II system the growth rate is conveniently substituted for the supersaturation. With the assumption that the degree of agitation is constant and that the effect of temperature changes on the nucleation constant is negligible, the nucleation rate in compartment i becomes

$$B_i = k_N * w_i * G_i^j. \tag{19}$$

Phenomena such as attrition, agglomeration, crystal breakage, and size-dependent crystal growth are neglected in this model for the sake of simplicity.

Crystal-size distribution — moments

In general the balance for the moment k over compartments 1, i, and N of a cascade of crystallizers can be written as

$$S_{k,1} + \frac{f * m_{k,2}}{\tau} - \frac{(1+f) * m_{k,1}}{\tau} = 0, \tag{20}$$

$$S_{k,i} + \frac{(1+f) * m_{k,i-1}}{\tau} + \frac{f * m_{k,i+1}}{\tau} - \frac{(1+2f) * m_{k,i}}{\tau} = 0, \tag{21}$$

$$S_{k,N} + \frac{(1+f) * m_{k,N-1}}{\tau} - \frac{(h+f) * m_{k,N}}{\tau} = 0, \tag{22}$$

with boundary condition $m_{3,i} = w_i / k_v$.

For the zeroth moment $m_{0,i}$, which indicates the number of crystals in compartment i, the source term $S_{k,i}$ is equal to the nucleation rate B_i (Eq. 18). For the higher moments $S_{k,i}$ is given by (Randolph and Larson, 1988):

$$S_{k,i} = k * G_i * m_{k-1,i}. \tag{23}$$

The mean crystal size and the coefficient of variation of the crystal-size distribution can be calculated from the moments of the crystal size distribution:

$$L_n = \frac{m_1}{m_0} \quad \text{and} \quad L_m = \frac{m_4}{m_3} \tag{24}$$

$$CV_n = \left(\frac{m_0 * m_2}{m_1^2} - 1\right)^{1/2} \quad \text{and} \quad CV_m = \left(\frac{m_3 * m_5}{m_4^2} - 1\right)^{1/2}. \tag{25}$$

Crystal size distribution — population density

The population balance for each compartment is similar to the moment equations (Eqs. 20–23) given by

$$G_1 * \frac{dn_1}{dl} + \frac{f * n_2}{\tau} - \frac{(1+f) * n_2}{\tau} = 0, \tag{26}$$

$$G_i * \frac{dn_i}{dl} + \frac{(1+f) * n_{i-1}}{\tau} + \frac{f * n_{i-1}}{\tau} - \frac{(1+2f) * n_i}{\tau} = 0, \tag{27}$$

$$G_8 * \frac{dn_8}{dl} + \frac{(1+f)n_7}{\tau} - \frac{(h+f) * n_8}{\tau} = 0, \tag{28}$$

with boundary condition $n_i(0) = B_i/G_i$, where B_i and G_i are obtained by solving the moment equations (Eqs. 20–23). The population densities in the eight compartments, $n(L)$, are calculated by using the fourth-order Runge-Kutta method.

Porosity and permeability of a crystal bed

The so-called geometrical method developed by Ouchiyama and Tanaka (1981, 1984) can be applied to calculate the porosity of the crystal bed constructed by random packing of particles with an arbitrary size distribution. This method is based on the coordination number C_n around each particle of size L. The input parameters for this porosity model are the size distribution and the porosity of a bed of uniform-sized crystals, ϵ_0.

The numerical form of the geometrical porosity model is given by

$$\epsilon = 1 - \frac{\sum_{k=1}^{\infty} L_k^3 * n_{i,k}}{\sum_{k=1}^{K} (L_k \sim L_{n,i})^3 * n_{i,k} + \frac{1}{C_n} * \sum_{k=1}^{K} \left[(L_k + L_{n,i})^3 - (L_k \sim L_{n,i})^3\right] * n_{i,k}} \tag{29}$$

where

$n_{i,k}$ = number of particles in size class k in compartment i [number/m^3]
L_k = particle size in class k
$L_{n,i}$ = number-based mean size in compartment i
K = total number of size classes
$L_k \sim L_{n,i} = 0$ for $L_k \le L_{n,i}$
$L_k - L_{n,i}$ for $L_k > L_{n,i}$

The averaged coordination number C_n is given by

$$C_n = 1 + \frac{4}{13} * (7 - 8 * \epsilon_0) * L_{n,i} * \left(\frac{\sum_{k=1}^{K} (L_k + L_{n,i})^2 * \left[1 - \frac{3}{8} * \left(\frac{L_{n,i}}{L_k + L_{n,i}}\right)\right] * n_{i,k}}{\sum_{k=1}^{K} \left[L_k^3 - (L_k \sim L_{n,i})^3\right] * n_{i,k}} \right). \tag{30}$$

From Eqs. 29 and 30 it is clear that porosity ϵ_i depends on the number-based mean size $L_{n,i}$ as well as on the first, second, and third moments of the CSD. In this approach, particles larger than $L_{n,i}$ are assumed not to affect the porosity.

The permeability of the crystal bed can now be calculated from the Kozeny-Carman equation:

$$P_{kc} = \frac{1}{K_{kc}} * \frac{\epsilon^3}{(1-\epsilon)^2} * \frac{1}{S_0^2}, \tag{31}$$

where

K_{kc} = Kozeny-Carman constant ($K_{kc} = 5$ for spheres)
S_0 = specific surface area of the particles (m^2/m^3)

MacDonald et al. (1991) suggested the following alternative:

$$P_m = \frac{1}{K_m} * \frac{\epsilon^3}{(1-\epsilon)^2} * (L_{2,1})^2 \tag{32}$$

where

K_m = MacDonald constant ($K_m = 9\pi^2/2 = 44.4$)
$L_{2,1}$ = length-based mean size (L_l)

Setup of the cascade of crystallizers with backmixing model

A flow chart of the CCB model is presented in Figure 4. Input to the heat and mass balances are practical operation

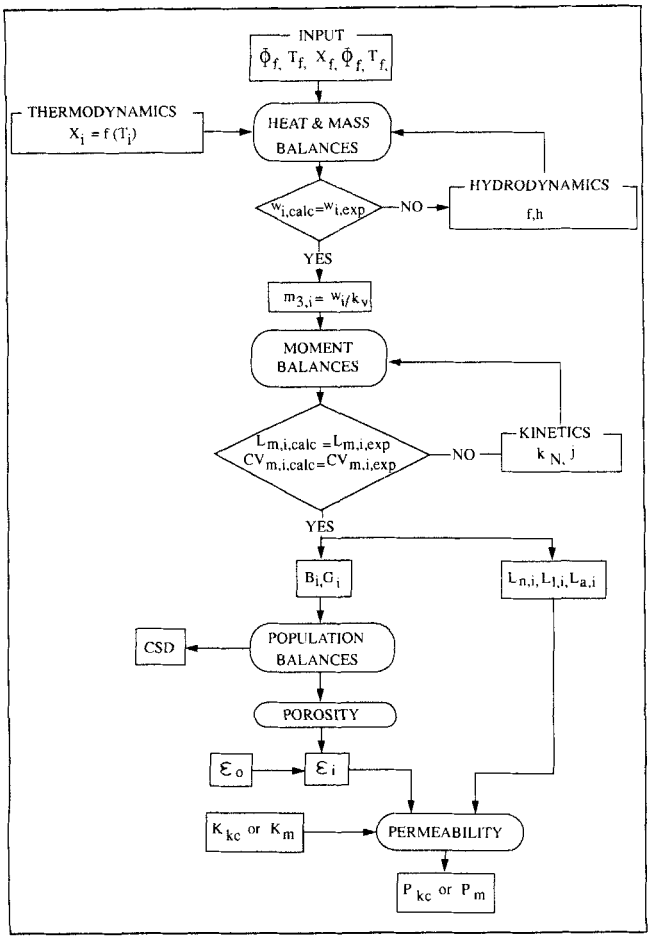

Figure 4. CCB model.

conditions, a relation for the liquidus, the backmix ratio f, and the classification ratio h. Both hydrodynamic parameters must be determined by fitting the calculated crystal content ($w_{i,\text{calc}}$) to experimental data ($w_{i,\text{exp}}$). Next, the crystal content (via $m_{3,i} = w_i/k_v$), the nucleation constant k_N, and the nucleation exponent j are input data to the CSD moment balances. Both kinetic parameters must be determined by fitting calculated and experimental values for the mass-based mean size L_m and coefficient of variation CV_m. At this point the nucleation rate, the growth rate, the mean size, and coefficient of variation can be calculated in each compartment. The full CSD can be calculated via the population balances. Next, the porosity and the permeability of a bed of crystals can be calculated. Calculation time amounts to approximately 4 min on a personal IBM-compatible computer with a 486 processor.

Experimental Procedure

The trough of the pilot plant CDC has a volume of 100 L, and it is divided into eight compartments. The seven cooling elements are connected in series and have a total wiped surface area of 0.91 m^2. The coolant flows countercurrent to the product from the seventh to the first cooling element. A mixture of caprolactam and water, from which caprolactam crystallized upon cooling, was used as the feed stock during the experiments.

Crystallization experiments were performed within the following limits:

Feed flow (Φ_f): 56.5–113 [L/h]
Water content feed stock: 1.0–7.6 [wt%]
Coolant flow (Φ_c): 125–500 [L/h]
Revolution rate discs: 15 [rpm]

In the startup phase of an experiment the inlet temperature of the coolant was gradually lowered until the crystal content in the overflow of the CDC reached the desired value (10–35 vol. %). To assure a steady-state operation, the crystallizer was operated for at least seven times the mean residence time after nucleation had occurred. The inlet temperature of the feed was kept just above its melting-point temperature. Slurry samples were taken from the overflow and seven sample points positioned at the bottom of the trough underneath the openings in cooling elements. As a result, a sample taken, for example, underneath the first cooling element was actually a mixture of the contents of the first and the second compartment.

The crystal size distribution was determined off-line using a laser diffraction technique. For this analysis, slurry samples were first centrifuged, and then the obtained crystals were suspended in a saturated n-decane solution. The bed permeability and the crystal content of a slurry sample were determined through filtration at a constant pressure difference (Coulson and Richardson, 1978). The permeability of the bed proved to be dependent on the applied pressure drop, indicating that the bed is compressible. The permeabilities reported in this article were obtained with an applied pressure drop of 0.2 bar. The water content of the liquid samples was determined through Karl-Fisher titration. The physical properties of the caprolactam/water feedstock, as used in the calculations, are presented in Table 1.

In addition to the crystallization experiments, a few tracer-pulse experiments were performed to verify the hydrodynamic model. The feedstock in these experiments was either a homogeneous water phase or a suspension of plastic particles (PVC) in water. A concentrated sodium chloride solution was used as tracer material.

Results

This section is divided into two parts. The first part covers the experimental optimization study and describes the effects of different operating conditions on the permeability of the crystals produced in the CDC. The second part deals with the modeling of the crystallization process in the CDC and

Table 1. Physical Properties of the Caprolactam/Water Mixture Used in the Calculations

Heat of crystallization (ΔH_m)	142 kJ/kg
Melting point (T_m)	342 K
Specific heat liquid phase ($C_{p,L}$)	2.13 kJ/kg·K
Specific heat solid phase ($C_{p,S}$)	1.67 kJ/kg·K
Viscosity	14–18 mPa·s
Specific weight ($\rho_L \approx \rho_S$)	1,000 kg/m^3
Slope liquidus (q)	345 K

Table 2. Effect of Process Conditions on the Product Permeability

Exp. Code	Φ_f L/h	Φ_c L/h	Water Content Feed wt. %	Crystal Content Compartment 8 vol. %	P_b 10^{-12} m^2	Remarks
18/03	56.5	500	2.2	26.5	36	Standard experiment
19/01	56.5	125	2.3	20.2	27	Effect of coolant flow
02/02	56.5	500	2.2	22.1	35	
11/03	56.5	500	2.3	11.6	17	Effect of residence time
16/03	113	500	2.4	11.8	11	
09/08	56.5	500	2.5	27.9	44	Effect of water content
01/04	56.5	500	7.6	27.8	21	

presents a comparison between model predictions and experimental results.

Throughout this section the results from experiment 18/03, which will be referred to as the *standard* experiment, are used to demonstrate observed trends, to fit the key parameters of the CCB model, and to compare model predictions with experimental findings.

Optimization of the permeability

The operating conditions and the main results of some experiments are summarized in Table 2. The crystal content and the permeability of the crystals in various compartments and in the overflow of the CDC during the standard experiment (18/03) are shown in Figure 5. The values of the *overflow* are registered on the horizontal axis in Figure 5 as *compartment number 8.5*.

Figure 5 shows a steady increase in the crystal content from the first to the last compartment, followed by a small decrease in the overflow. This trend has been observed in all experiments. The permeability shows a gradual increase, particularly in the second half of the CDC. In experiments with a lower crystal content in the CDC (≤ 15 vol. % in compartment 8), the permeability did not change significantly in the CDC. The increase of the permeability in experiment 18/03 was not accompanied by a significant change in the mass-based CSD, as can be seen in Figure 6 ($L_m \approx 370$ μm, $CV_m \approx 0.48$).

The *crystal content* in the CDC was found to have a dominant effect on the permeability of the product crystals. In

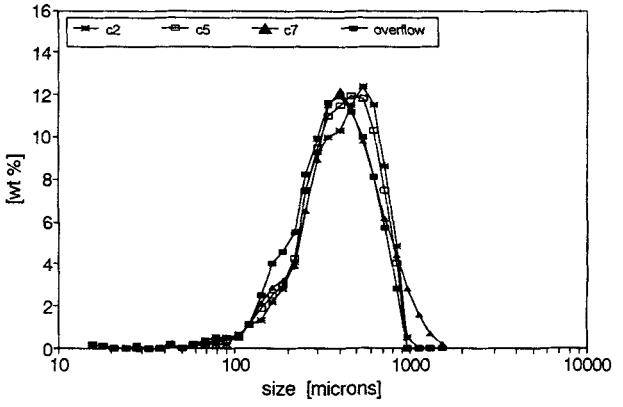

Figure 6. Mass-based crystal-size distributions of slurry samples taken from compartments 2, 5, and 7, and overflow during experiment 18/03.

Figure 7 the permeability of the crystals in the overflow is plotted as a function of the crystal content in the eighth compartment of the CDC for all experiments. An increase in the crystal content clearly has a positive effect on the permeability. The large variations in permeability between the different experiments could not be correlated to changes in the measured (mass-based) CSD. In all experiments: 330 μm $\leq L_{m,\text{product}} \leq 370$ μm and $0.45 \leq CV_m \leq 0.55$ (the differences are within the range of reproducibility).

An increase in the *coolant flow* from 125 to 500 L/h also had a positive impact on the product permeability, as can be seen in Table 2. Experiments 19/01 and 02/02 were per-

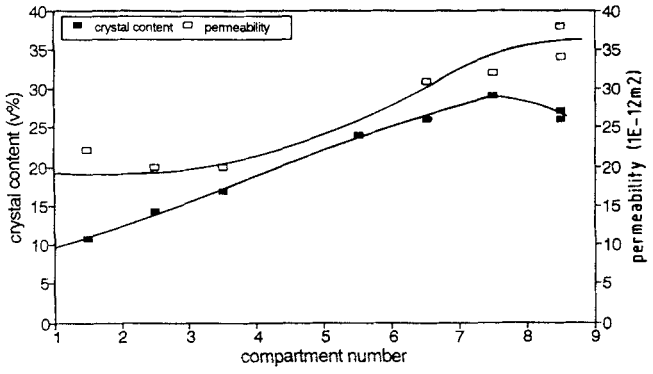

Figure 5. Permeability and crystal content in the CDC during the standard experiment (18/03).

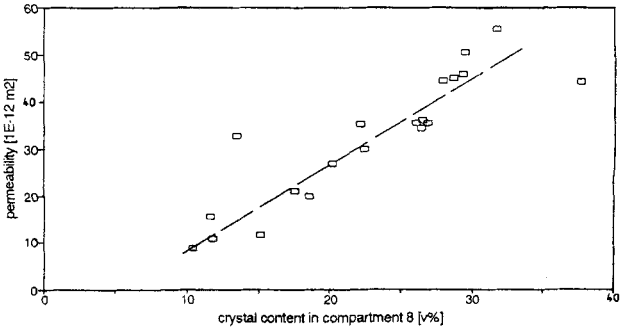

Figure 7. Product permeability vs. crystal content in compartment 8.

formed under the same operating conditions except for the coolant flow (Φ_c). Another benefit of the high coolant flow proved to be a reduction in the degree of encrustation on the unwiped parts of the cooling elements.

The *residence time*, which could be adjusted through the feed flow, proved to have a beneficial effect on the product permeability (Table 2). Comparison of experiments 11/03 and 16/03, both performed at a low crystal content, shows a small increase in permeability upon an increase in the residence time.

An increase in the *water concentration* in the feed from 2.5 to 7.6 wt. % resulted in a significant reduction in the product permeability (see Table 2, experiments 09/08 and 01/04). No significant effect of the water concentration was observed upon variation from 1 to 2.5 wt. %.

The effect of crystallization conditions on the *morphology* of caprolactam crystals has also been investigated; the results are presented elsewhere (Jansens, 1994; Jansens et al., 1994). The morphology of the crystals formed in the CDC proved not to depend on the operating conditions (within the experimental limits) nor on the compartment number, and therefore crystal morphology cannot explain the observed changes in permeability.

Modeling of the crystallization process

The CCB model contains four key parameters: the backmix ratio f, the classification ratio h, the nucleation constant k_N, and the nucleation exponent j. The hydrodynamic parameters (f,h) must be determined by fitting the calculated to the measured crystal content, and the kinetic parameters (k_N and j) must be determined by fitting the calculated to the predicted mass-based mean size and coefficient of variation (see also Figure 4).

Hydrodynamics and Crystal Production. The BC model described well the residence time distribution of the sodium chloride tracer pulse in the CDC both with the homogeneous water phase and with the slurry of PVC particles and water. Figure 8 shows a comparison of the experimentally determined $E(t)$ and the prediction of the BC model. The backmix ratio ($f = 2$) was obtained using Eq. 3. Figure 8 demonstrates that the BC model offers a good description of the

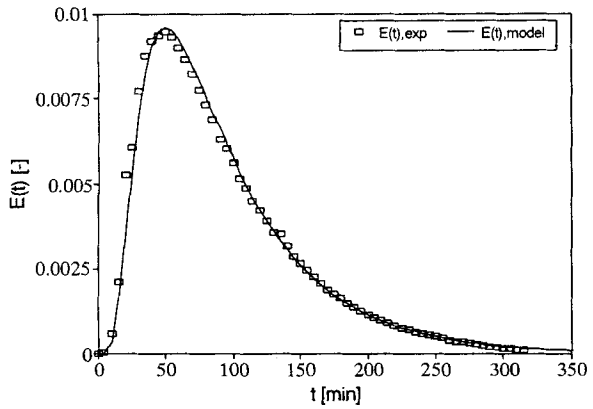

Figure 8. $E(t)$ curves for CDC at 15 rpm and 60 L/h with a homogeneous water phase ($f = 2$).

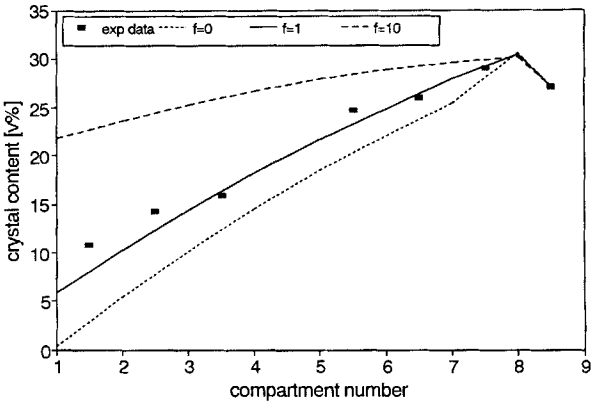

Figure 9. Measured vs. simulated crystal content in CDC for different backmix ratios (f) for experiment 18/03.

hydrodynamic behavior of a homogeneous liquid phase in the CDC. Other tracer-pulse experiments revealed that the backmix ratio increases with increasing revolution rate and decreasing flow rate.

To avoid pollution of the caprolactam/water feedstock, no tracer-pulse experiments were performed during the crystallization test runs. In this case the classification ratio h was determined by Eq. 4, and the backmix ratio f was obtained by fitting the simulation result of the CCB model to the experimental data on the crystal content in the CDC.

Figure 9 shows the data of the standard experiment (18/03) and simulation results for $f = 0$ (no backmixing), $f = 1$, and $f = 10$ (nearly ideal mixing), where $h = 0.91$. The simulation result for $f = 1$ shows good agreement with the experimental result, particularly for compartments 3 to 8. The experimental curve is somewhat flatter for the first compartments (1 to 3) than for the simulation curve, which indicates larger backmixing on this side of the CDC. Probably the local backmix ratio in the CDC is dependent on the crystal content, which affects the apparent slurry viscosity, whereas f is assumed to be a constant throughout the CDC in the CCB model. In order to investigate this effect, h and f are plotted as a function of the crystal content in the last compartment of the CDC (Figure 10). The plot demonstrates that with the increasing crystal content in the CDC, the classification in the last compartment becomes negligible and the degree of backmixing becomes less.

It is concluded that the CCB model, based on the BC approach, provides a simple and satisfactory description of the hydrodynamic behavior and the crystal production in a cascade of crystallizers.

Crystallization kinetics and crystal size distribution. Different combinations of k_N and j result in a good match between the simulation results and the experimental mass-based CSDs, that is, $j = 1.5$ and $k_N = 2.5 \times 10^{19}$, $j = 2$ with $k_N = 1.3 \times 10^{23}$, and $j = 3$ with $k_N = 3.5 \times 10^{30}$. For the standard experiment (18/03), Figure 11 presents the experimentally determined L_m and CV_m and their simulated values for $j = 2$ (and $k_N = 1.3 \times 10^{23}$). The differences between the simulated L_m and CV_m for different j–k_N combinations are too small to be able to distinguish between these combinations. There are, however, distinct differences in the calculated L_n and

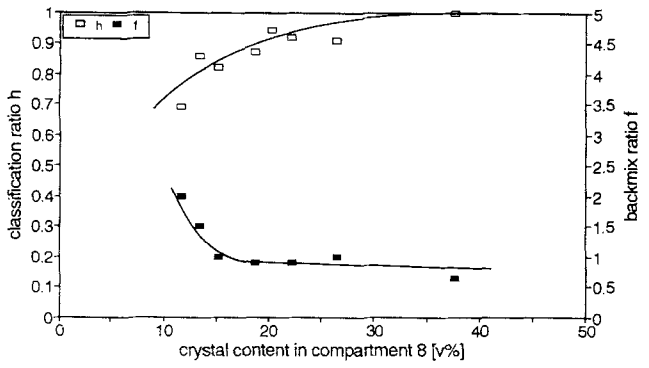

Figure 10. Dependence of backmix ratio *f* and classification ratio *h* on the crystal content in the overflow of CDC (different experiments).

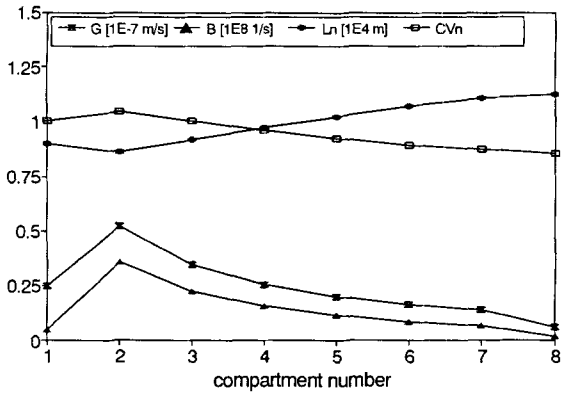

Figure 12. Calculated growth rate (*G*), nucleation rate (*B*), number-based mean size (L_n), and coefficient of variation in CDC for experiment 18/03.

CCB parameters: $f = 1$, $h = 0.9$, $k_N = 1.3 \times 10^{23}$, $j = 2$.

CV_n. The simulations with higher j values result in a steeper increase in the number-based mean diameter L_n throughout the CDC and a smaller value of CV_n in the overflow of the CDC. Unfortunately, transformation of the measured *mass-based* CSDs into *number-based* CSDs is subject to large errors and does not provide accurate data on L_n or CV_n. It is therefore impossible at this stage to positively discriminate between the different nucleation exponents. It will be shown below that the CCB prediction of the permeability depends on the choice of j, which offers an opportunity to select the best j value.

For the operating conditions of the standard experiment, Figure 12 presents the growth rate G, the nucleation rate B, L_n, and CV_n in different compartments of the CDC as calculated with the CCB model for $j = 2$. The rates B_i and G_i show a strong increase from the first to the second compartment, followed by a gradual decrease to the last compartment. Note that the first compartment of the CDC is cooled only on one side, and part of the available cooling power is used to cool the (slightly overheated) feedstock to its melting temperature. The choice of the nucleation exponent j has only a minor effect on G_i. With increasing j values, nucleation occurs more and more in the first compartments of the CDC. The increase in the number-based mean size L_n and the narrowing of the number-based CSD ($CV_n <$) with increasing compartment number indicate a reduction of the number of small crystals (fines), which explains the measured increase in the permeability along the CDC (Figure 5).

Figure 13 presents the CCB predictions for L_n and CV_n in the overflow vs. the experimentally determined product permeability for different experiments. It is shown that the CCB model predicts a large value of L_n and a small value of CV_n for experiments that yielded a high product permeability. Therefore the calculated values of L_n and CV_n already provide a qualitative indication of the product permeability.

CCB permeability predictions. In Figure 14, the CCB permeability predictions based on the Kozeny-Carman relation (Eq. 31) and on the MacDonald relation (Eq. 32) are compared with the measured data for the standard experiment (18/03). Both model predictions show correct trends, but the absolute values are either too high (P_m) or too low (P_{kc}). The values of the constants K_{kc} and K_m must be adjusted to get a better agreement between the absolute values ($K_{kc} = 3.3$ and $K_m = 57.7$). It is very difficult to decide on the best permeability prediction (Kozeny-Carman or MacDonald). Be-

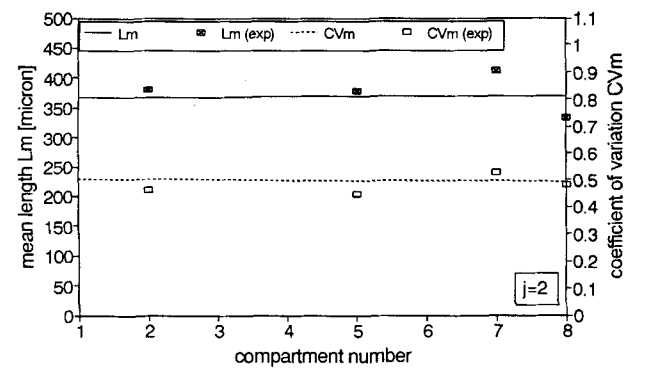

Figure 11. Measured and calculated mass-based mean size (L_m) and coefficient of variation (CV_m) for experiment 18/03.

CCB parameters: $f = 1$, $h = 0.9$, $k_N = 1.3 \times 10^{23}$, $j = 2$.

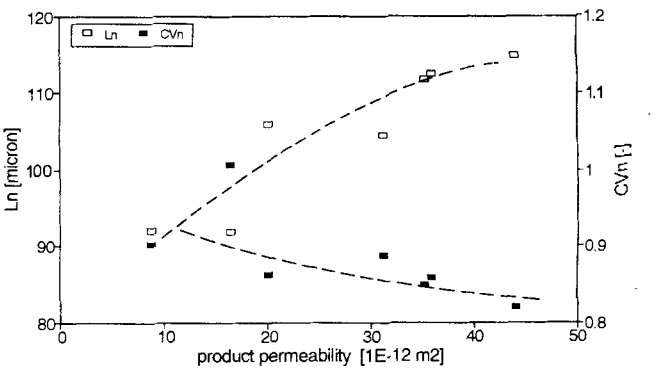

Figure 13. Calculated number-based mean size (L_n) and coefficient of variation (CV_n) vs. measured product (overflow) permeabilities for different experiments.

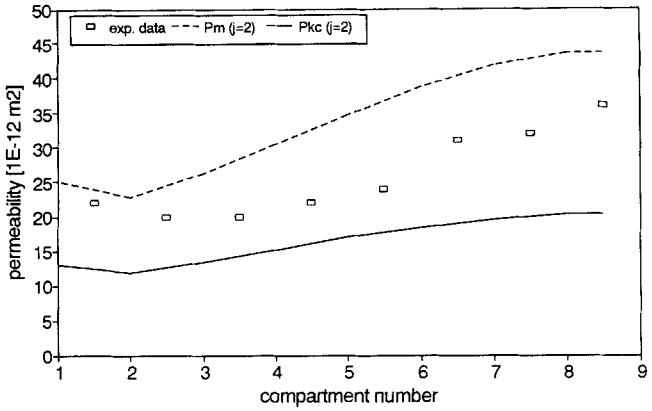

Figure 14. CCB predictions (P_{kc} & P_m) and measured permeabilities in different compartments of CDC for the standard experiment (18/03).

CCB parameters: $f = 1$, $h = 0.9$, $k_N = 1.3 \times 10^{23}$, $j = 2$, $K_{kc} = 5$, $K_m = 44.4$.

cause the MacDonald equation is more sensitive to changes in the smaller size classes, it is used below.

The effect of the choice of j (and k_N) on the permeability prediction is clearly shown in Figure 15. The permeability curves, obtained with $K_m = 57.7$, are steeper at higher values of j. From Figure 15 it can be concluded that the combination of $j = 2$ with $k_N = 1.3 \times 10^{23}$ yields the best agreement with the experimental data.

In Figure 16, CCB predictions of the permeability of the *product* crystals in the *overflow*, based on the MacDonald relation using $K_m = 57.7$, are plotted vs. the values measured during different experiments. The agreement between the predicted and the measured values is not perfect but at this stage acceptable.

Discussion

The mass-based CSD did not change significantly throughout the CDC and proved to be almost independent of the

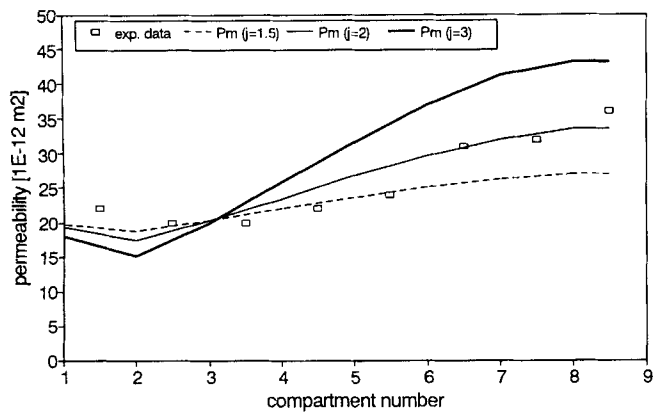

Figure 15. Effect of the choice of kinetic parameters (k_N and j) on the permeability predictions of the CCB model (P_m, experiment 18/03).

CCB parameters: $f = 1$, $h = 0.9$, $K_m = 57.7$; $k_N = 2.5 \times 10^{19}$ with $j = 1.5$; $k_N = 1.3 \times 10^{23}$ with $j = 2$; $k_N = 3.5 \times 10^{30}$ with $j = 3$.

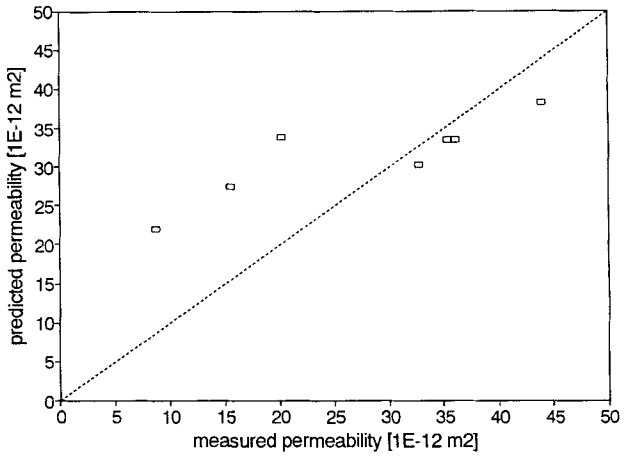

Figure 16. Comparison between CCB prediction (P_m with $K_m = 57.7$) and measured permeabilities in the overflow of CDC for different experiments.

CCB parameters: $K_m = 57.7$, $k_N = 1.3 \times 10^{23}$ with $j = 2$.

residence time and other operating conditions, which indicates that nucleation as well as backmixing play a dominant role with respect to crystal growth in the CDC. The nucleation rate (and the growth rate) decreases with higher crystal content, which explains the positive effect of an increase in the crystal content of the product permeability. A positive side effect of an increase in the crystal content is the reduction of the amount of backmixing, which results in a better approximation of the plug flow in the CDC, and consequently in a narrowing of the CSD.

At a high coolant flow (500 L/h) the temperature difference between the coolant and the slurry decreases from the first to the last compartment. This "converging" temperature profile results in relatively low nucleation rates in the last compartments of the CDC, which explains the positive effect of a high coolant flow on the product permeability. At 125 L/h coolant flow the temperature profile was almost parallel or even diverging, resulting in a higher nucleation rate toward the exit of the CDC and lower permeabilities.

The raising of the water content from 2.5 to 7.6 wt. % resulted in an increase in the liquid viscosity from 14 to 18 mPa·s due to the formation of hydrogen bonds. The growth rate is probably hampered by the viscosity increase (Jansens, 1994). The permeability of a crystal bed appears to be governed by the number-based rather than by the mass-based CSD. The mass-based CSD is insensitive to the presence of small crystals, whereas these fines have a significant effect on the bed porosity. Besides nucleation, crystal breakage and attrition also contribute to the production of fines. It may be useful to incorporate source terms for these phenomena in the CSD equations, but the introduction of extra constants, which must be determined, reduces the value of the model as an engineering tool.

Conclusions

The filterability/permeability of caprolactam crystals produced in the cooling disc crystallizer (CDC) depends mainly on the crystal content. An increase in the crystal content de-

creases the degree of backmixing and reduces the nucleation rate, both of which have a positive impact on the product filterability. Other operating conditions that proved to have an effect on the filterability are the coolant flow, the water content, and the residence time.

The developed cascades of crystallizers with backmixing model (CCB model) provides a satisfactory prediction of the production, size distribution, and permeability of the crystals produced in the CDC and can be used to optimize the operating conditions.

Notation

A = cooling surface area [m^2]
C_p = specific heat [kJ/kg·K]
F = modified backmix ratio
k_v = volumetric shape factor
K = heat transfer coefficient [$kW/m^2 \cdot K$]
l = length [m]
t = time [s]
T_m = melting point temperature [K]
x = fraction of the main component in liquid phase [kg/kg]

Greek letters

ΔH_m = heat of crystallization [kJ/kg]
ΔT = temperature difference between bulk and coolant [K]
ρ = specific weight [kg/m^3]
τ = mean residence time [s]
σ = variance of the residence time distribution [s]

Subscripts

a = surface area based
i = compartment number i
l = length based
m = mass based
n = number based
p = product

Literature Cited

Bell, R. L., and A. L. Babb, "On the Extension of the Method of Moments to a Cascade of Well-Mixed Discrete Stages with Back-Flow between Stages," *Chem. Eng. Sci.*, **20**, 1001 (1965).

Coulson, J. M., and J. F. Richardson, *Chemical Engineering*, Pergamon, New York (1978).

Garside, J., and M. B. Shah, "Crystallization Kinetics from MSMPR Crystallizers," *Ind. Eng. Chem. Process Des. Dev.*, **10**, 509 (1980).

Jansens, P. J., and G. M. van Rosmalen, "Fractional Crystallisation," *Handbook on Crystal Growth*, Vol. 2(A), Chap. 6, D. T. J. Hurle, ed., Elsevier, Amsterdam, in press (1994).

Jansens, P. J., Y. Langen, E. P. G. van den Berg, and R. M. Geertman, "The Morphology of Caprolactam Crystals under Different Crystallization Conditions," *J. Cryst. Growth*, submitted (1994).

Jansens, P. J., "Fractional Suspension Crystallization of Organic Compounds," PhD Thesis, Delft Univ. of Technology, Delft Univ. Press, Delft, The Netherlands (1994).

Klinkenberg, A., "Moments of Residence Time Distributions for Cascades of Stirred Vessels with Backmixing," *Chem. Eng. Sci.*, **23**, 175 (1968).

MacDonald, M. J., C. F. Chu, P. P. Guillot, and K. M. Ng, "A Generalized Blake-Kozeny Equation for Multisized Spherical Particles," *AIChE J.*, **37**(10), 1583 (1991).

Ouchiyama, N., and T. Tanaka, "Porosity of a Mass of Solid Particles Having a Range of Sizes," *Ind. Eng. Chem. Fund.*, **20**(1), 71 (1981).

Ouchiyama, N., and T. Tanaka, "Porosity Estimation for Random Packings of Spherical Particles," *Ind. Eng. Chem. Fund.*, **23**, 490 (1984).

Randolph, A. D., and M. A. Larson, *Theory of Particulate Processes*, 2nd ed., Academic Press, San Diego (1988).

Roemer, M. H., and L. D. Durbin, "Transient Response and Moments Analysis of Backflow Cell Model for Flow Systems with Logitudinal Mixing," *Ind. Eng. Chem. Fund.*, **6**(1), 121 (1967).

Van der Laan, E. Th., "Notes on the Diffusion-Type Model for the Logitudinal Mixing in Flow (O. Levenspiel and W. K. Smith)," *Chem. Eng. Sci.*, **7**, 187 (1958).

Zief, M., and W. R. Wilcox, *Fractional Solidification*, Dekker, New York (1967).

Manuscript received Feb. 28, 1994, and revision received Apr. 22, 1994.